Title: Discordant K-Ar and Young Exposure Dates for the Windjana sandstone, Kimberley, Gale Crater, Mars

Current list of authors: P. M. Vasconcelos[1*], K. A. Farley[2], C. A. Malespin[3,4], P. Mahaffy[3], D. Ming[5], S. M. McLennan[6], J.A Hurowitz[6], Melissa S. Rice[7]

Affiliations:
[1]School of Earth Sciences, The University of Queensland, Brisbane, Queensland, QLD 4072
[2]Division of Geological and Planetary Sciences, California Institute of Technology, Pasadena, CA, 91125; farley@gps.caltech.edu
[3]NASA Goddard Space Flight Center, Greenbelt, MD, 20771
[4]Universities Space Research Association, Columbia, MD, 21046
[5]NASA Johnson Space Center, Houston, TX, 77058
[6]Department of Geosciences, State University of New York, Stony Brook, NY, 11794
[7] Geology and Physics/Astronomy Departments, Western Washington University, Bellingham, WA 98225

Key points:

• In situ K-Ar dating of two aliquots of a sanidine-rich sandstone on Mars yield disparate results (627±50 and 1710±110 Ma)

• Discordant KAr ages suggest incomplete Ar extraction and possible sample heterogeneity

• Cosmogenic ^{3}He, ^{21}Ne and ^{36}Ar ages for sanidine-rich sandstone suggest recent (<100 Ma) exposure history

This article has been accepted for publication and undergone full peer review but has not been through the copyediting, typesetting, pagination and proofreading process which may lead to differences between this version and the Version of Record. Please cite this article as doi: 10.1002/2016JE005017

© 2016 American Geophysical Union. All rights reserved.

Abstract

K-Ar and noble gas surface exposure age measurements were carried out on the Windjana sandstone, Kimberley region, Gale Crater, Mars using the Sample Analysis at Mars instrument on the Curiosity rover. The sandstone is unusually rich in sanidine, as determined by CheMin X-ray diffraction, contributing to the high K_2O concentration of 3.09±0.20 wt % measured by APXS analysis. A sandstone aliquot heated to ~ 915°C yielded a K-Ar age of 627±50 Ma. Reheating this aliquot yielded no additional Ar. A second aliquot heated in the same way yielded a much higher K-Ar age of 1710±110 Ma. These data suggest incomplete Ar extraction from a rock with a K-Ar age older than 1710 Ma. Incomplete extraction at ~900°C is not surprising for a rock with a large fraction of K carried by Ar-retentive K-feldspar. Likely variability in the exact temperature achieved by the sample from run to run, uncertainties in sample mass estimation, and possible mineral fractionation during transport and storage prior to analysis may contribute to these discrepant data. Cosmic ray exposure ages from ^{3}He and ^{21}Ne in the two aliquots are minimum values given the possibility of incomplete extraction. However, the general similarity between the ^{3}He (57±49 and 18±32 Ma, mean 30 Ma) and ^{21}Ne (2±32 and 83±24 Ma, mean 54 Ma) exposure ages provides no evidence for under-extraction. The implied erosion rate at the Kimberley location is similar to that reported at the nearby Yellowknife Bay outcrop.

Index terms: Planetary and lunar geochronology, Cosmogenic-nuclide exposure dating, Radioisotope geochronology

Keywords: Mars, K-Ar, ^{3}He, ^{21}Ne, ^{36}Cl, sanidine

1. Introduction

Remote geochronology on Mars, using the complementary geochemical, mineralogical, and isotopic capabilities of the Mars Science Laboratory (MSL), has provided valuable information on Martian geology and morphological evolution [Farley et al., 2014]. In situ K-Ar dating of the Cumberland sample of the Sheepbed lacustrine mudstone of the Yellowknife Bay formation yielded a K-Ar age of 4.21 ± 0.35 Ga. This age is consistent with estimates derived from crater densities in the source terrane on the crater rim, and it suggests that the detrital minerals in the mudstone record the age of the original Martian crust before the impact that created Gale Crater. The old K-Ar result implies that the detrital phases were not significantly altered after deposition.

© 2016 American Geophysical Union. All rights reserved.

The consistency between the measured K-Ar age and the expected age of the source terrane provides confidence in the accuracy of the unexpected results obtained from cosmogenic isotope exposure ages. Concentrations of ^{3}He, ^{21}Ne, and ^{36}Ar produced by cosmic ray interactions with elements in the uppermost few meters of the Martian crust provide exposure ages of 72 ± 15, 84 ± 28, and 79 ± 24 Ma, respectively, for the Cumberland sample [Farley et al., 2014]. The concordant but young results reveal an active geomorphological evolution, where scarp retreat by aeolian erosion promotes the progressive unroofing of Gale Crater sedimentary beds. Quantifying this active erosion history is important in the reconstruction of the infilling and excavation history of Gale Crater [Grotzinger et al., 2015], and it is particularly important in the search for organic biosignatures. As the presently rarefied Martian atmosphere offers little protection from solar radiation and cosmic ray bombardment, organic molecules in the near surface may be degraded if exposed for more than a few millions of years [Dartnell, 2011; Grotzinger et al., 2014; Hassler et al., 2014; Pavlov et al., 2014]. Active scarp retreat, as revealed by the youthful exposure ages, suggests that the bases of recently eroded scarps are attractive candidate sites for preservation of organic molecules [Farley et al., 2014].

After the successful dating campaign at Cumberland, the MSL team identified a butte and associated scarp in the Kimberley area (-4.64 °N, 137.4 °E), along the rover's path towards Mt Sharp, as a promising site for a second drilling campaign, including further geochronology and search for organic molecules (Figures 1, 2). Three distinct geological units identified from orbital imagery coexist at the Kimberley site: the Hummocky Plains unit and the Kimberley formation Rugged and Striated units (Figure 2a) [Grotzinger et al., 2015]. Locally, the more resistant Rugged unit caps three topographic mounds, one of which, Mt Remarkable, was targeted for drilling (Figure 2a). The cross-stratified sandstone (Dillinger member) at the base of Mt Remarkable was the last unit sampled for geochronology before crossing the boundary between stratigraphic units derived from erosion of the northern crater rim [Bradbury group) that blanket the crater floor (Aeolis Palus) and stratigraphic units (Murray formation) that form the base of Mt Sharp (Aeolis Mons) (Figure 1). Reliable K-Ar and exposure ages for the Kimberley formation might help to constrain the stratigraphic succession of the Gale crater sediments and provide further information about sediment sources. Exposure ages for the Kimberley sediments should further constrain the history of denudation of the crater, revealing if the sediments at the base of Mt Remarkable were indeed

© 2016 American Geophysical Union. All rights reserved.

recently exposed and therefore likely to preserve any organic compound against degradation by radiation.

2. Sample and Methodology

The Rugged and Striated units crop out through the overlying Hummocky unit in the Kimberley area, forming a series of buttes (Figure 2a). The Kimberley formation sediments sit ~35 meters topographically and stratigraphically above the Sheepbed mudstone investigated and dated close to the landing site (Figure 1, insert) [Grotzinger et al., 2015]. The butte chosen for the drilling campaign is surrounded by an apron of the Rugged unit, while more deeply dissected areas reveal outcrops of the Striated unit (Figure 2a). The sedimentary strata that constitute the Rugged and Striated units, the Kimberley formation, are subdivided into five members, as illustrated in Figure 2b. They range, from bottom to top, from breccio-conglomerates at the base (Point Coulomb member), planar bedded and very coarse sandstones containing granules (Liga member), south-dipping faintly-laminated sandstones (Square Top member), cross-stratified sandstones (Dillinger member), and the butte-forming massive sandstone (Mt Remarkable member) [Le Deit et al., 2015; Grotzinger et al., 2015; Treiman et al., 2016]. A flat slab of the Dillinger member, named Windjana, was selected for drilling and geochronology (Figures 2a,d). Mars Hand Lens Imager (MAHLI) observations of the Windjana outcrop, drill-hole walls and spoils, and sample dump reveal a granular texture and a dark and more reddish color for this sandstone (Figures 3c,d), when compared to the Cumberland sediments dated at Yellowknife Bay.

A preliminary mini-drill campaign (sol 615) for rock properties and stability deemed the Windjana site suitable for full-depth drilling (Figure 3a-c). The sample used for geochronology was recovered from the full drill undertaken in the central area of the large Windjana sandstone block (sol 621), centered atop an obvious fracture (Figure 3a). Sample drilling and ingestion through the powder acquisition drill system followed standard MSL procedures, where rock cuttings were obtained by rotary percussion drill from a 1.6 cm diameter and 5 cm deep drill-hole [Anderson et al., 2012]. The upper 1.5-2 cm of the drilled powder was deposited on the outcrop, and only powdered rock from below 1.5-2 cm travelled up the auger in the drill arm and into the chamber for delivery to the Collection and Handling for Interior Martian Rock Analysis (CHIMRA) processing unit. Movement of the powder through CHIMRA is driven by gravity and vibration, and sample powders delivered to CHIMRA were sorted through a 150-μm sieve [Anderson et al., 2012; Mahaffy et al., 2012].

© 2016 American Geophysical Union. All rights reserved.

The sub-150 μm fraction was mixed and stored within CHIMRA for multiple analyses by SAM and CHEMIN and, after dumping on the ground, by APXS.

Rietveld refinement of Chemin results (acquired during sols 623-632) for an aliquot of the Windjana sample reveals, in decreasing order of abundance, the presence of augite, sanidine, magnetite, pigeonite, smectite/illite, olivine, oligoclase, andesine, fluorapatite, hematite, ilmenite, bassanite, anhydrite, pyrrhotite, akaganeite, and possible traces of labradorite, enstatite, jarosite, and kaolinite (Table 1) [Treiman et al., 2016]. The sample also contains 15 wt% X-ray amorphous material. The large proportion of sanidine, tentatively identified as detrital sanidine but also consistent with a diagenetic feldspar structure [Treiman et al., 2016], is unique among samples so far investigated at Gale Crater, and it contributes to the rock's high K content (3.09 ± 0.20 (2σ)) wt% K_2O) [Treiman et al., 2016]. The high proportions of magnetite and phyllosilicates, interpreted either as authigenic phases formed after sediment deposition [Treiman et al., 2016] or as detrital components [Le Deit et al., 2016], are also peculiar to the Windjana sample and have significant implications for noble gas retentivity and cosmogenic isotope production.

Two sets of APXS analyses are available for the Windjana sample [Thompson et al., 2016; Treiman et al., 2016]. On sol 622, APXS analyzed the tailings derived from the upper 1.5-2 cm of the drill hole (Figure 3b,c), revealing a K_2O content of 3.65 wt% [Thompson et al., 2016; Treiman et al., 2016]. On sol 704, the sample remaining in CHIMRA was discarded and analyzed on the ground (Figure 3d), revealing a K_2O content of 3.09 ± 0.20 (2σ) wt% K_2O (Table 2) [Treiman et al., 2016]. Since the first analysis corresponds to a fraction of the drill-hole not ingested by CHIMRA, we choose the second as more relevant for computing geochronology results by integration with the noble gas analyses obtained by SAM.

2.1 Noble gas analysis

Two different aliquots of the <150 μm sample powder were delivered from CHIMRA to SAM for noble gas isotopic analysis. The two aliquots, Windjana 1 (WJ1) and Windjana 2 (WJ2), represent two nominally equivalent fractions of homogenized powder drilled on sol 621. Given the slight differences in sample handling and major differences in results, we describe the analytical procedures separately.

© 2016 American Geophysical Union. All rights reserved.

As described in greater detail in Farley et al. [2014], a 75 mm^3 portioning tube at the outlet of CHIMRA was filled with the <150 μm powdered sample, which was delivered to the SAM quartz cup via a funnel [Anderson et al., 2012; Mahaffy et al., 2012]. A triple portion of each sample (225 mm^3) was estimated to correspond to a mass of 135 ± 18 mg using the same probabilistic model for mass delivery as the one used for the Cumberland sample. As the sample delivery procedures were the same for Cumberland, WJ1 and WJ2, we assume a similar mass for all three samples.

Before sample delivery, the quartz cups were preconditioned at 900 °C; after sample delivery, the cups were pre-heated to ~135 °C in He gas flow to expel any adhering volatiles. A major distinction between the two Windjana aliquots and the previously successful Cumberland experiment is that the Cumberland sample was heated in pyrolysis Pyro-1 oven, while both Windjana samples were heated in Pyro-2 oven (Figure 4) [Mahaffy et al., 2012]. In Pyro-2 oven the temperature sensing wire present in Pyro-1 oven is replaced by a second heater wire, potentially enabling the sample to be heated to a higher temperature. However, the absence of a sense wire limits direct knowledge of actual oven temperature achieved during gas extraction. As discussed below, this uncertainty and our inability to realize the heating time and sample temperature required for full ^{40}Ar extraction likely contribute to our inability to secure complete Ar release from this sample.

Before heating the quartz cup and sample, the manifold and QMS were pumped through the wide range pumps (WRP1 and WRP2) (Figure 4) for ~15 minutes, after which the system background was measured in dynamic mode. Next, the sample cup was slowly pre-heated to ~ 135°C for 20 minutes with a He carrier gas to drive off adsorbed or weakly bound volatiles. After this initial outgassing step, the pumps are turned off, and the valve to the zeolite CO_2 scrubber was opened prior to slowly heating the sample to an estimated temperature of ~ 915±15^{o}C; samples were kept at temperature for 25 min. In the absence of a sense wire, the sample temperature was estimated based on current delivered to the heater wire and a laboratory calibration (see below). Evolved gases were cleaned of active species by H_2O and CO_2 scrubbers and a SAES ST172 getter, which had been conditioned prior to this run. While samples were being heated, the valves to the quadrupole mass spectrometer (V11, V12), and the valve to the hydrocarbon and noble gas traps (V44) were closed, while the valves isolating the oven from the scrubbers and getter were open, allowing the gas extracted to be scrubbed and cleaned of active species during heating. The scrubbing and gettering

© 2016 American Geophysical Union. All rights reserved.

procedures lasted for 1 hr 45 min, after which the gas was analyzed initially in dynamic mode in the QMS, which is equipped with a second SAES ST172 getter that had also been activated before this experiment. After a period of analysis in dynamic scan, constriction of the high conductance valve, HC1, venting the mass spectrometer enabled analysis in the high sensitivity semi-static mode [Farley et al. 2014, Supplementary Material]. Full static-mode analysis in SAM was not carried out in this experiment to avoid overpressure in the mass spectrometer. A useful procedural modification at the end of the Windjana analyses, as compared to the Cumberland sample, was the pumping of the entire manifold, including the QMS, while the QMS was still in scanning mode. This step enables direct measurement of the background in semi-static mode.

After puzzlingly low ^{40}Ar results were obtained on the first extraction of noble gases from WJ1 (Figure 5a), this same aliquot was reheated to determine whether any additional noble gases could be extracted. For this experiment, Windjana 1 re-extract (WJ1-RE) (Figure 5b), the sample temperature was designed to be slightly higher (i.e., the voltage in the wire was increased by 0.5 V) than the temperature reached in the first heating experiment (915±15 ^{o}C). The evolved gas was then analyzed by the same procedures outlined above. Whether a higher temperature was actually achieved is difficult to ascertain, but the results suggest that the second step did not achieve a higher temperature, as discussed below.

A second 135±18 mg <150 μm aliquot (WJ2) from the same original drill-hole and kept in CHIMRA until sol 763 was delivered to a new quartz cup in Pyro-2 oven and analyzed following the exact same procedures carried out during the analyses of the WJ1-RE sample, including the 25 min and slightly higher voltage sample degassing step aiming at T > 915±15 ^{o}C (Figure 5c).

3. Results

3.1 Noble Gas Quantification and Age Calculations

The analytical results for the noble gases (m/z 3, 21, 36, and 40) and other m/z of interest (2, 20, 38, and 39) are illustrated in Figure 5. Signal intensities during sample pre-heating, dynamic analysis, semi-static analysis, pump-out period, and background analysis permit visualizing the dynamics of gas liberation during sample pre-heating, gas evolution during both dynamic and semi-static analytical modes, effectiveness of gas pump-down during

© 2016 American Geophysical Union. All rights reserved.

sample venting, and the background values for m/z of interest. The experiment also permits visualizing instability periods immediately following valve opening and closing, and the settle-down periods before signal stabilization.

The focus of our noble gas investigation is a segment of the semi-static experiment in which the signal intensities are stable enough for quantification (Figures 5, 6). During this period, m/z 40 remains nearly invariant while m/z values representing more active gases (HCl, hydrocarbons, water) decline (Figure 6). Data reduction procedures followed the steps outlined in Farley et al. [2014], where signals in the stabilized periods were corrected for deadtime, each measurement in the stabilized period was corrected by a mean background value, and all m/z values were corrected for isobaric interferences. In addition, 32 kcps were subtracted from the final computed m/z 40 results to account for a hot blank previously measured on Mars for the SAM oven [Farley et al., 2014]. The mean signal and standard deviations for each m/z were computed and translated into abundances using sensitivities (295, 69, and 41 cps.pmol^{-1} for Ar, Ne, and He, respectively) also previously obtained for the SAM instrument [Farley et al., 2014]. Tabulated uncertainties were computed using a Monte Carlo method that includes uncertainties in peak heights, isobar correction factors, and instrumental sensitivities. Uncertainty in mass, common to all concentration and age determinations, is included separately to facilitate assessment of the internal consistency of the surface exposure ages.

The stabilized interval used for each of the three runs and the resulting noble gas concentrations are listed in Table 4. K-Ar ages were computed using the decay constants of Renne et al. [2010]. Cosmogenic production rates at the Mars surface were computed from the APXS elemental abundance data (Table 2) following previous procedures [Farley et al., 2014]. The resulting values, listed in Table 3, are similar to those from the CB sample except for ^{36}Ar. The ^{36}Ar production rate in Windjana is substantially lower than in CB owing to the lower concentration of its parent, the high neutron-capture cross-section element Cl, in Windjana (see Farley et al., 2014]).

© 2016 American Geophysical Union. All rights reserved.

Table 3 reveals discrepant K-Ar ages from the two Windjana aliquots, 627±50 and 1710±110 Ma. The re-extraction experiment on the first aliquot did not yield additional Ar.

Cosmogenic ^{36}Ar concentrations in the Windjana samples are highly uncertain owing to the extremely high concentration of isobaric HCl present during the semi-static analyses. ^{3}He and ^{21}Ne concentrations have better precision than ^{36}Ar, but are less precise than obtained on the Cumberland sample, again owing to uncertainties in the isobaric corrections. No meaningful cosmogenic isotope concentrations could be computed from the re-extraction experiment. Using the estimated Mars surface production rates (Table 3), the ^{3}He exposure ages for WJ1 and WJ2 are, respectively, 57±49 and 18±32 Ma, the ^{21}Ne ages are 2±32 and 83±24 Ma, and the ^{36}Ar ages are 65±104 and 60±144 Ma (Table 3). An error weighted mean age of just the spallation isotopes (^{3}He and ^{21}Ne) is 46 ±16 Ma; including neutron-capture-produced ^{36}Ar does not change this result significantly (46 ±15 Ma).

4. Discussion

The most striking result of these experiments is the unexpectedly young and irreproducible K-Ar ages. The Gale Crater plain (Aeolis Palus) blanketed by the sedimentary sequence hosting the Windjana samples has a well constrained crater-count age of ~3.4-3.2 Ga [Grant et al., 2014; Grotzinger et al., 2015]. In addition, detrital sanidine, the most volumetrically significant K-bearing phase, is likely derived from alkaline igneous rocks in the northern Gale Crater rim [Treiman et al., 2016], the same source terrain as the 4.2 Ga Cumberland sample. Therefore, the minimum ages of the sedimentary sequence and of the potential detrital mineral source rocks make the ~1 Ga K-Ar age implausible. More puzzling, the measured difference in age between WJ1 and WJ2 is far larger than we can readily explain. Thus we conclude some sort of issue occurred that could be related to the completeness of the extraction, sorting of grains during sample procession or other factors. In this section we attempt to identify and evaluate possible candidates. For this purpose it is useful to understand how K is housed in the rock.

© 2016 American Geophysical Union. All rights reserved.

4.1 The K-bearing phases

There are two competing interpretations for the chemical and mineralogical composition of the Windjana samples. The first, based on the combination of chemical analysis by the APXS instrument and Rietveld refinement of ChemMin X-ray diffraction data, suggests that 100% of the K occurs in detrital sanidine and oligoclase, with a possible minor contribution from detrital plagioclase and authigenic jarosite [Treiman et al., 2016]. An alternative model, based on newly calibrated ChemCam data, proposes that detrital sanidine, anorthoclase, and illite (formed during the alteration of the source rocks prior to erosion) are responsible for the high K contents at Windjana [Le Deit et al. 2016]. These competing models have distinct implications for the interpretation of the K-Ar data.

Most obviously, if 20 ± 3 wt% of the total mass is a disordered K-feldspar (structurally sanidine) with a composition of $Or_{95\pm2}Ab_{5\pm2}$ [Treiman et al., 2016], than sanidine must dominate the K_2O content of the Windjana sample that we dated. In fact, 20 ± 3 wt% sanidine of $Or_{95\pm2}Ab_{5\pm2}$ composition would result in 3.06 ± 0.15 wt% K_2O in the sample, accounting for ~100% of the 3.09 ± 0.20 wt% K_2O measured by APXS for the dump pile, the material most likely to represent the samples apportioned into SAM for EGA and geochronology. This precludes the presence of any other K-bearing phase in the sample, either crystalline, poorly crystalline, or amorphous. This interpretation is consistent with the relatively small proportion of oligoclase (2 wt%) and plagioclase (2 wt%) and the K-depleted nature of other significant mineral components (plagioclase, olivine, augite, pigeonite, magnetite), which preclude these detrital phases as significant contributors to the K budget. Phyllosilicates, tentatively identified as illite or collapsed smectites, were initially interpreted as potential K-sources. The K-deficit resulting from the presence of 20 ± 3 wt% sanidine, however, also precludes the presence of K-rich illite, leading Treiman et al. [2016] to interpret that only Mg-Fe collapsed smectites are present. For the same reason, no K-rich phase is interpreted to occur in the 15 wt% amorphous material. The only other K-bearing phase tentatively identified in the ChemMin XRD results is jarosite, which, if present, occurs in trace amounts and hosts very little K and radiogenic Ar.

© 2016 American Geophysical Union. All rights reserved.

If sanidine and oligoclase are the dominant K-bearing phases in WJ1 and WJ2, their origin is relevant in the interpretation of the geochronological results. Sanidine is most abundant in extrusive acid igneous rocks [Deer et al., 1966], it occurs in pegmatites [Pecora, 1942] and hydrothermal alteration zones [Cerny and Chapman, 1986], and it is also a relatively common product of diagenetic reactions in sedimentary sequences [Baskin, 1956; Kastner and Siever, 1979; Woodward, 1972]. For the Windjana sediments, Treiman et al. [2016] favor an extrusive igneous source rock, as briefly summarized below.

The abundance of fresh olivine, pyrrhotite, and K-poor amorphous material in the Windjana sediments argues against an *in situ* diagenetic original for the K-feldspars [Treiman et al., 2016]. The absence of detrital quartz and carbonates also argues against the erosion of a diagenetically altered sedimentary precursor. The absence of detrital quartz, amphiboles, micas, chlorite, serpentines, epidote, and other common metamorphic or hydrothermal phases at Windjana precludes a hydrothermal or pegmatitic origin for sanidine [Treiman et al., 2016]. Therefore, sanidine is interpreted as a detrital phase derived from erosion of an alkaline basaltic igneous rock exposed at the northern crater rim [Treiman et al., 2016]. Furthermore, the coexistence of sanidine with olivine, augite, pigeonite, and plagioclase at Windjana suggests a complex assemblage of igneous source rocks (mafic and felsic) at the northern crater rim [Treiman et al., 2016; Thompson et al., 2016]. Lastly, the coexistence of sanidine, olivine, augite, pigeonite, and plagioclase together with the presence of detrital pyrrhotite argues against significant weathering at the source [Treiman et al., 2016].

Le Deit et al. [2016], on the other hand, suggest that the ChemCam analyses confirm the presence of K-feldspar, possibly sanidine and anorthoclase, but those analysis also suggest the presence of K-bearing phyllosilicates, such as illite, if one assumes that sanidine is not as K-rich ($Or_{95\pm2}Ab_{5\pm2}$) as interpreted by Treiman et al. [2016]. Le Deit et al. [2016] prefer to interpret that K-enrichment in the Windjana samples results from the presence of detrital sanidine, anorthoclase, and illite, and that the significant detrital illite component would suggest partial alteration of the source rocks.

© 2016 American Geophysical Union. All rights reserved.

Nevertheless, if detrital sanidine is the major [Treiman et al., 2016] or a significant [Le Deit et al., 2016] K-bearing phase in the Windjana sample, its grain size distribution would affect the release of Ar during the heating step in the K-Ar experiment. As outlined and illustrated in Treiman et al. [2016], MAHLI image 0612MH0003880010203325C00 shows that the sediments drilled at Windjana are composed of sand grains that average ~ 100 μm across, with only the occasional presence of grains as large as 400 μm across, and a large proportion of grains <80 μm. It is likely that the harder and more chemically resilient detrital phases (e.g., sanidine, augite) comprise the coarser sand-size fraction.

4.2 Assessing the effect of mass loss during sample loading

In the absence of a mechanism for directly weighing samples on Mars, the only way to estimate the mass of sample analyzed for geochronology is through volumetric and density estimation. In the MSL Sample Transfer Model, the efficacy of transfer of a sample powder from a 76 mm^3 portioning tube into the SAM oven cup is assessed by evaluating the results of 130 repeat experiments conducted on sample powders under Mars conditions [Farley et al., 2014]. In the present study, if the masses delivered to the quartz cup varied significantly from the estimated 135±18 mg, it could partially lead to some age discrepancy. Variable wind gusts could, in principle, result in sample loss during delivery from the portioning tube into the SAM cup, despite the fact that MSL is equipped with "wind guards" [Anderson et al., 2012] to obviate this problem.

In the K-Ar age equation, age varies with ln ($1/^{40}K$), where the ^{40}K content is the mass-dependent parameter. Consequently, age is rather insensitive to variations in mass. For example, even if it is assumed that 80% of the WJ2 sample mass was "blown in the wind", the estimated age for the amount of ^{40}Ar measured would be ~ 2.85 Ga, still much lower than the expected ~ 4.2 Ga result. Therefore, error in sample mass estimation is not a likely cause for the unexpectedly young and disparate K-Ar results.

4.3 Mineral unmixing

The fine-grained texture of the Windjana sandstone, combined with the fact that it is composed of a mixture of detrital and authigenic minerals of distinct grain sizes and hardness, suggests that particle-size sorting could have occurred during drilling [Anderson et al., 2012]. The harder detrital phases (e.g., pyroxene, sanidine) may have produced a coarser grained powder than the phyllosilicates and the X-ray amorphous components. If so, it is easy to

© 2016 American Geophysical Union. All rights reserved.

envisage that sample unmixing can occur. Once processed through the 150 μm sieve, the sample is stored within a compartment in CHIMRA to source aliquots to SAM and Chemin [Anderson et al., 2012]. Sample manipulation procedures aim to optimize effective mixing of the cached sample. Because CHIMRA is located on the robotic arm, both driving and turret manipulation act to shake, vibrate, and possibly stir the sample, which could in special circumstances lead to unmixing of coarse and fine particles. Sample transfer through CHIMRA and ultimate delivery to the quartz cups in SAM is also achieved through shaking and vibration [Mahaffy et al., 2012]. An aliquot is taken from this compartment by tipping it upward, which causes gravity feed into a sampling tube. Ultimately the residual sample is tipped and dumped onto the surface of Mars.

If the relative abundance of K-bearing phases varies among SAM-analyzed aliquots, or between the SAM aliquots and the final dump-pile from which sample chemistry was derived, erroneous and irreproducible K-Ar results could be obtained. The flow of granular materials in the Mars environment is notoriously hard to model or simulate, so evaluating this possibility in any quantitative way is difficult.

The most significant effect of unmixing, however, may be to exacerbate the effects of incomplete noble gas extraction, as discussed below.

4.4 The Temperature Dependence of Noble Gas Extraction Efficiency

Incomplete Ar extraction from the sample offers an additional and more plausible explanation for the anomalous K-Ar ages. If so, the amount of un-extracted Ar must be large and very different for the two samples. For the sake of comparison, if the Windjana sample was coeval with the Cumberland sample [Farley et al., 2014] we would have measured a signal of 3.2 Mcps of ^{40}Ar. However, in WJ1 we actually measured just 0.17 Mcps, or approximately 5.2 % of the expected signal. Similarly, for WJ2 we obtained just ~ 19% of the expected signal.

© 2016 American Geophysical Union. All rights reserved.

Bogard [2009] predicted, based on incremental heating analysis of K-bearing phases from Nakhlites and Shergottites, that incomplete ^{40}Ar extraction from plagioclase and pyroxene would pose the greatest challenge for dating samples in situ on Mars. At ~ 900°C, plagioclases from Nakhlites may release 80-85 wt% of the total Ar content, while plagioclase from Shergottites only release ~30-40 wt% of the total argon. At 900°C, pyroxenes from either type of meteorite only release negligible amounts of argon, but are a minor host for K. Sanidine, which was detected in Northwest Africa 7034 meteorite [Agee et al., 2013) but had not been directly detected on Mars until the Curiosity mission XRD analysis of the Windjana sandstone, is even more argon retentive. During K-Ar analysis, total argon extraction from sanidine is difficult to achieve due its high retentivity to noble gases [McDougall and Harrison, 1999], relatively high (~ 1250 °C) melting temperatures and the high viscosity (η = 10^5 Pa.s^{-1}) of the melts produced, which retain argon in bubbles, preventing its complete release. Often, temperatures in excess of 1400°C must be achieved for complete Ar extraction [Cassata and Renne, 2013]. Incremental-heating analysis of representative terrestrial sanidine, orthoclase, and perthite samples, ranging from 0.1-1 mm in diameter, only diffuse about 5-10 wt% of their radiogenic argon content at a temperature of ~900 °C, even after prolonged (> 17 hours) heating [Cassata and Renne, 2013], so the magnitude of the observed effect in Windjana is not unreasonable. Power limitations on the SAM noble gas release experiment preclude such long extraction times.

Our WJ1 re-extraction experiment was designed specifically to test this hypothesis, on the grounds that reheating of a sample that retains ~80-95% of its Ar is expected to yield additional Ar when reheated to the same or higher temperature. Thus the failure to measure any additional Ar in the re-extract experiment was unexpected, provided the sample actually attained a higher or equivalent temperature. A possibility that accounts for this failure, and which has potentially also contributed to the discrepancy in Ar yield between the two aliquots, was identified after these experiments were completed. In the absence of a sense wire, the temperature of Pyro-2 oven is established by regulating the current to the heater wire. However, there are additional electrical loads in this circuit that consume power, possibly in a way that varies among runs. Thus one way to account for all of these observations is that the temperature was too low to ensure complete extraction, and owing to uncertainties decreased in the order WJ2>WJ1>WJ1-RE.

© 2016 American Geophysical Union. All rights reserved.

A complementary explanation, and a more important effect if unmixing occurred during sample ingestion or storage in CHIMRA, would be the separation of the ingested sample into a coarser fraction rich in detrital K-feldspars (WJ1) and a fine-grained fraction richer in authigenic illite/smectite and amorphous components (WJ2). The two unmixed aliquots would respond quite differently to heating, enhancing differences in the efficacy of noble gas extraction from the two samples, potentially producing the large discrepancy in K-Ar ages obtained for WJ1 and WJ2.

A related possibility is that flux-assisted melting has degassed some but not all of the sample. Volatile constituents (e.g., S, Cl, water, F, Li) may act to lower the melting point of mineral grains within the sample, promoting Ar release. If so, an additional possible explanation for the lack of Ar in the re-extraction of WJ1 is that the flux was entirely consumed in the first extraction, and the remaining mineral grains are too retentive to diffuse Ar at all at ~900^{o}C. Differences in compositions and grain sizes between WJ1 and WJ2 could also have contributed to differences in the efficacy of flux melting between the two samples.

4.5 Exposure Ages

Given the strong evidence for incomplete argon extraction, it is possible that the cosmogenic noble gases were also only partially released. The temperature at which noble gases are released from minerals generally increases in the order He<Ne<Ar. Thus one prediction of incomplete extraction is that the degree of incompleteness is likely to increase in the same order. As a consequence, the exposure ages in an incomplete extraction situation would likely decrease from He to Ne to Ar. The error-weighted means of the two aliquots of the ^{3}He, ^{21}Ne, and ^{36}Ar exposure ages are respectively 30±27 Ma, 54±19 Ma, and 63±84 Ma. These are all within uncertainty and, if anything, increase (rather than decrease) with noble gas atomic number. Thus there is no strong evidence to support (nor refute) incomplete cosmogenic noble gas extraction. Note that it is possible to have incomplete ^{40}Ar extraction and (mostly) complete ^{3}He, ^{21}Ne, and ^{36}Ar extraction because they originate from different elements and so will reside in different minerals (e.g., argon-retentive sanidine hosts a large fraction of the ^{40}Ar but a far smaller fraction of ^{3}He and ^{21}Ne, and essentially no ^{36}Ar). Despite the lack of evidence for incomplete extraction, it seems prudent to consider these exposure ages as lower limits.

© 2016 American Geophysical Union. All rights reserved.

Exposure ages from the nearby Sheepbed mudstone averaged ~78 Ma for all three isotopes, each of which was determined with substantially better precision than obtained here. By using the different depth profile of spallation and neutron-capture production, Farley et al. [2014] were able to constrain the style of erosion occurring at Yellowknife Bay, favoring a scarp-retreat model that rapidly exposed the outcrop from depths greater than a few meters. The large uncertainties in the present data set preclude a similar level of interpretation. Taken at face value, the Windjana cosmogenic isotope data can be interpreted equally well as: A) retreat of a few meter-high scarp, possibly the one now defining the butte to the west of the drilled outcrop (Figure 2), at 46 ±15 Ma; or B) vertical erosion occurring at a mean rate of about 1.5 $cm.Ma^{-1}$. As described by Farley et al. [2014], these end-member scenarios are not unique; for example, vertical erosion can be episodic and reburial can occur. In addition, if we have not completely extracted the cosmogenic gases, then the age of scarp retreat may be too young and the mean erosion rate too high. Given these caveats we find no evidence indicating very different erosion rates or styles between the Yellowknife Bay and Kimberley drill sites.

4.6 The Way Forward

The possibility of incomplete gas extraction at the maximum temperatures achievable by the SAM ovens (900-1100°C) poses challenges to future *in situ* MSL geochronological experiments, particularly when dating coarse-grained sedimentary units. Therefore, future drilling campaigns for geochronology, if targeting detrital sedimentary units, should focus on very fine-grained sediments (mudstones) similar to those successfully dated at Cumberland [Vaniman et al., 2014], where sample grain size and composition (high Na-Ca-Mg) may favor flux-fusion.

Alternatively, the geochronological capabilities of SAM could be better utilized by dating authigenic minerals. As the rover climbs Mt Sharp, a series of clay mineral-, oxide-, and sulfate-rich units will be encountered [Fraeman et al., 2013; Golombek et al., 2012; Grotzinger et al., 2015]. Minerals in parts of these units are likely to be mostly authigenic and associated with the diagenesis and subsequent alteration of lacustrine sediments or evaporites possibly coeval and interstratified with the Bradbury group fluvial sediments dated at Yellowknife Bay and Kimberley [Fraeman et al., 2013; Grotzinger et al., 2015]. Authigenic clay minerals, oxides and sulfates from Mt Sharp units provide ideal targets for dating the Martian water cycle, an important step in characterizing the history of atmospheric evolution

© 2016 American Geophysical Union. All rights reserved.

[Mahaffy et al., 2015] and habitability of early Mars [Grotzinger et al., 2014; Grant et al., 2014]. Clay mineral formation likely records the peak of humid periods, when pervasive weathering or diagenesis of sedimentary units resulted in the precipitation of sedimentary clays [Bristow et al., 2015]. Sulfates, on the other hand, likely record the transition towards aridity, when evaporation of the Gale lake and dehydration of the sediments resulted in sulfate deposition. The very late-stage sulfates deposited in conspicuous [Léveillé et al., 2014; Nachon et al., 2014] veins may record the final stages of water movement through a lucustrine deposits in a dehydrating sedimentary pile and planet. K-bearing authigenic clays (illite, chloritized smectite, collapsed smectites), oxides (hollandite, birnessite, todorokite) and sulfates (jarosite and alunite), if present in Mt Sharp, provide ideal targets for MSL K-Ar geochronology because these phases completely release their argon contents at temperatures below 1000 °C (~1000 °C for illite [Hassanipak and Wampler, 1996]), 400-800 °C for Mn oxides [Vasconcelos, 1999] and 400-700 °C for jarosite and alunite [Waltenberg, 2012], obviating the difficulties encountered with incomplete argon extraction for the K-feldspar-rich Windjana sediments. Exploring for these phases and targeting a drilling campaign towards sampling authigenic clays and K-bearing oxides or sulfates may, therefore, optimize current SAM's geochronological capabilities to answer fundamental questions on the evolution of the water cycle on Mars.

On the other hand, if targeting pure authigenic phases is not feasible, a mixed detrital-authigenic sample may still yield reasonable geochronological results if the sample can be dated in two steps. A first heating step at 800°C would extract most of the argon from authigenic minerals, without extracting argon from detrital phases (assuming no detrital clays or sulfates), particularly if the detrital component consists of K-feldspars and plagioclase. A subsequent step at 1000°C might succeed in extracting the gas from the detrital component, particularly if flux melting occurs. The gas extracted from the first step would determine the age of the authigenic phases, while the second step would reveal the age of the detrital component. The major challenge in the two-step approach would be to apportion K between the detrital vs. the authigenic components, which will require robust determinations of mineral abundance and chemical compositions for each fraction.

© 2016 American Geophysical Union. All rights reserved.

5. Conclusions

Geochronological results for two aliquots of the Windjana cross-bedded sandstone drilled at the base of Mt Remarkable, Kimberley, Gale Crater, Mars, yield two disparate and unreasonably low K-Ar ages (627±50 and 1710±110 Ma) that are best explained as the result of incomplete noble gas extraction. Incomplete argon extraction may have resulted from the high retentivity of the main argon-bearing mineral at Windjana (K-feldspar) and the relatively low heating temperatures achieved with the SAM oven (~900°C). The disparate apparent ages obtained for the two aliquots of the drilled sample probably result from incomplete and differential argon extraction as samples may have been heated to slightly different temperatures. In addition, potential sample fractionation by granular flow during storage between sampling and analyses may have fractionated relative mineral abundances and/or grain sizes, exacerbating differences in incomplete gas extraction. A less likely conclusion, given that it is not clear from mineralogical analysis that the Windjana sediments contain any K in clay minerals, is that the young results reflect preferential dating of authigenic illite; the disparate ages could simply record the relative proportions of K-bearing clays in each sample aliquot. In any case, the oldest age obtained (1710 ± 110 Ma) represents a minimum K-Ar age for the source rocks from which the K-rich sediments were derived. In contrast to the K-Ar results, compatible noble gas exposure ages of 57±49 and 18±32 Ma (^{3}He), 2±32 and 83±24 Ma (^{21}Ne), and 65±104 and 60±144 Ma (^{36}Ar) for the two aliquots tentatively suggest near-complete extraction of these noble gases, implying a young exposure history for the Windjana site.

Acknowledgements

The authors thank the Mars Science Laboratory Project teams for an effective and successful mission. Some of this research was carried out at the Jet Propulsion Laboratory, California Institute of Technology, under a contract with the National Aeronautics and Space Administration. Data presented in this paper are archived in the Planetary Data System (pds.nasa.gov)

© 2016 American Geophysical Union. All rights reserved.

References:

Agee, C.B., Wilson N.V., McCubbin F.M., Ziegler K., Polyak V.J., Sharp Z.D., Asmeron Y., Nunn M.H., Shaheen R., Thiemens M.H., Steele A., Fogel M.L., Bowden R., Glamoclija M., Zhang Z., Elardo S.M., **Unique meteorite from early Amazonian Mars: water-rich basaltic breccia Northwest Africa 7034**, *Science*, 339, 780-783, 2013.

Anderson, R.C., L. Jandura, A.B. Okon, D. Sunshine, C. Roumeliotis, L.W. Beegle, J. Hurowitz, B. Kennedy, D. Limonadi, S. McCloskey, M. Robinson, C. Seybold, and K. Brown, **Collecting samples in Gale crater, Mars; an overview of the Mars Science Laboratory Sample Acquisition, Sample Processing and Handling System**, *Space Science Reviews*, 170:57-75, doi:10.1007/s11214-012-9898-9, 2012. [🕮]

Baskin Y., A study of authigenic feldspars, The Journal od Geology, 64(2): 132-155, 1956.

Bogard D.D., **K-Ar dating of rocks on Mars: Requirements from Martian meteorite analyses and isochron modeling**, *Meteoritics and Planetary Science*, 44(1):3-14, 2009

Bristow, T.F., D.L. Bish, D.T. Vaniman, R.V. Morris, D.F. Blake, J.P. Grotzinger, E.B. Rampe, J.A. Crisp, C.N. Achilles, D.W. Ming, B.L. Ehlmann, P.L. King, J.C. Bridges, J.L. Eigenbrode, D.Y. Sumner, S.J. Chipera, J.M. Morookian, A.H. Treiman, S.M. Morrison, R.T. Downs, J.D. Farmer, D. Des Marais, P. Sarrazin, M.M. Floyd, M.A. Mischna, and A.C. McAdam, **The origin and implications of clay minerals from Yellowknife Bay, Gale crater, Mars**, *American Mineralogist*, 100(4): 824-836, doi:10.2138/am-2015-5077, 2015. [🔓]

Cassata, W.S., and Renne, P.R., **Systematic variations of argon diffusion in feldspars and implications for thermochronometry**, *Geochimica et Cosmochimica Acta*, 112: 251-287, 2013.

Cerny P. and Chapman R., **Adularia from hydrothermal vein deposits: extremes in structural state**, *Canadian Mineralogist*, 24: 717-728, 1986.

Dartnell, L.R., **Ionizing Radiation and Life**, *Astrobiology*, 11(6): 551-582. doi:10.1089/ast.2010.0528.

Deer W.A., Howie R.A., and Zussman J., **Rock-forming minerals**, 4, Longmans, Lond. 1966.

Farley, K.A., C. Malespin, P. Mahaffy, J.P. Grotzinger, P. Vasconcelos, R.E. Milliken, M. Malin, K.S. Edgett, A.A. Pavlov, J.A. Hurowitz, J.A. Grant, H.B. Miller, R. Arvidson, L. Beegle, F. Calef, P.G. Conrad, W.E. Dietrich, J. Eigenbrode, R. Gellert, S. Gupta, V. Hamilton, D.M. Hassler, K.W. Lewis, S.M. McLennan, D. Ming, R. Navarro-González, S.P. Schwenzer, A. Steele, E.M. Stolper, D.Y. Sumner, D. Vaniman, A. Vasavada, K. Williford, R.F. Wimmer-Schweingruber, and the MSL Science Team, **In situ radiometric and exposure age dating of the Martian surface**, *Science*, 343(6169), 1247166, doi:10.1126/science.1247166, 2014. [🔓] [🔓] [🕮]

© 2016 American Geophysical Union. All rights reserved.

Fraeman A.A., R.E. Arvidson, J.G. Catalano. J.P. Grotzinger, R.V. Morris, S.L. Murchie, K.M. Stack, D.C. Humm, J.A. McGovern, F.P. Seelos, K.D. Seelos, and C.E. Viviano, **A hematite-bearing layer in Gale Crater, Mars: Mapping and implications for past aqueous conditions**, *Geology*, 41(10): 1103-1106, doi:10.1130/G34613.1., 2014.

Golombek, M., J. Grant, D. Kipp, A. Vasavada, R. Kirk, R. Fergason, P. Bellutta, F. Calef, K. Larsen, Y. Katayama, A. Huertas, R. Beyer, A. Chen, T. Parker, B. Pollard, S. Lee, Y. Sun, R. Hoover, H. Sladek, J. Grotzinger, R.Welch, E. Noe Dobrea, J. Michalski, and M. Watkins, **Selection of the Mars Science Laboratory landing site**, *Space Science Reviews*, 170:41-737, doi:10.1007/s11214-012-9916-y, 2012. [ ]

Grant, J.A., S.A. Wilson, N. Mangold, F. Calef III, and J.P. Grotzinger, **The timing of alluvial activity in Gale crater, Mars**, *Geophysical Research Letters*, 41(4):1142-1149, doi:10.1002/2013GL058909, 2014. [🕮]

Grotzinger, J.P., **Habitability, taphonomy, and the search for organic carbon on Mars**, *Science*, 343[6169): 386-387, doi:10.1126/science.1249944, 2014a. [💣] [💣] [🕮]

Grotzinger, J.P., D.Y. Sumner, L.C. Kah, K. Stack, S. Gupta, L. Edgar, D. Rubin, K. Lewis, J. Schieber, N. Mangold, R. Milliken, P.G. Conrad, D. DesMarais, J. Farmer, K. Siebach, F. Calef III, J. Hurowitz, S.M. McLennan, D. Ming, D. Vaniman, J. Crisp, A. Vasavada, K.S. Edgett, M. Malin, D. Blake, R. Gellert, P. Mahaffy, R.C. Wiens, S. Maurice, J.A. Grant, S. Wilson, R.C. Anderson, L. Beegle, R. Arvidson, B. Hallet, R.S. Sletten, M. Rice, J. Bell III, J. Griffes, B. Ehlmann, R.B. Anderson, T.F. Bristow, W.E. Dietrich, G. Dromart, J. Eigenbrode, A. Fraeman, C. Hardgrove, K. Herkenhoff, L. Jandura, G. Kocurek, S. Lee, L.A. Leshin, R. Leveille, D. Limonadi, J. Maki, S. McCloskey, M. Meyer, M. Minitti, H. Newsom, D. Oehler, A. Okon, M. Palucis, T. Parker, S. Rowland, M. Schmidt, S. Squyres, A. Steele, E. Stolper, R. Summons, A. Treiman, R. Williams, A. Yingst, and MSL Science Team, **A habitable fluvio-lacustrine environment at Yellowknife Bay, Gale Crater, Mars**, *Science*, 343(6169), 1242777, doi:10.1126/science.1242777, 2014b. [💣] [💣] [🕮]

Grotzinger, J.P., S. Gupta, M.C. Malin, D.M. Rubin, J. Schieber, K. Siebach, D.Y. Sumner, K.M. Stack, A.R. Vasavada, R.E. Arvidson, F. Calef III, L. Edgar, W.F. Fischer, J.A. Grant, J. Griffes, L.C. Kah, M.P. Lamb, K.W. Lewis, N. Mangold, M.E. Minitti, M. Palucis, M. Rice, R.M.E. Williams, R.A. Yingst, D. Blake, D. Blaney, P. Conrad, J. Crisp, W.E. Dietrich, G. Dromart, K.S. Edgett, R.C. Ewing, R. Gellert, J.A. Hurowitz, G. Kocurek, P. Mahaffy, M.J. McBride, S.M. McLennan, M. Mischna, D. Ming, R. Milliken, H. Newsom, D. Oehler, T.J. Parker, D. Vaniman, R.C. Wiens, and S.A. Wilson, **Deposition, exhumation, and paleoclimate of an ancient lake deposit, Gale crater, Mars**, *Science*, 350(6257):aac7575, doi:10.1126/science.aac7575, 2015. [□] [□] [ ]

Hassanipak A.A. and Wampler J.M., **Radiogenic argon released by stepwise heating of glauconite and illite: the influence of composition and particle size**, *Clays and Clay Minerals*, Vol. 44, No. 6, 717-726, 1996.

Hassler, D.M., C. Zeitlin, R.F. Wimmer-Schweingruber, B. Ehresmann, S. Rafkin, J.L. Eigenbrode, D.E. Brinza, G. Weigle, S. Böttcher, E. Böhm, S. Burmeister, J. Guo, J. Köhler, C. Martin, G. Reitz, F.A. Cucinotta, M.-H. Kim, D. Grinspoon, M.A. Bullock, A.

© 2016 American Geophysical Union. All rights reserved.

Posner, J. Gómez-Elvira, A. Vasavada, J.P. Grotzinger, and the MSL Science Team, **Mars' surface radiation environment measured with the Mars Science Laboratory's Curiosity rover**, *Science*, 343(6169), 1244797, doi:10.1126/science.1244797, 2014. [🔓] [🔓] [🕮]

Kastner M. and Siever R., **Low temperature feldspars in sedimentary rocks**, *American Journal fo Science*, 279: 435-479, 1979.

Le Deit, L., Mangold, N., Forni, O., D. Blaney, A. Cousin, G. Dromart, C. Fabre, M. Fisk, O. Gasnault, N. Lanza, J. Lasue, S. Le Mouélic, S. Maurice, M. Nachon, W. Rapin, M. Rice, V. Sautter, S. Schröder, D. Sumner, R. C. Wiens, **The potassic sedimentary rocks in Gale Crater, Mars as seen by ChemCam on board Curiosity**, 46th Lunar and Planetary Science Conference (2015), 1438.pdf, 2015.

Le Deit, L., N. Mangold, O. Forni, A. Cousin, J. Lasue, S. Schro□der, R.C. Wiens, D. Sumner, C. Fabre, K.M. Stack, R.B. Anderson, D. Blaney, S. Clegg, G. Dromart, M. Fisk, O. Gasnault, J.P. Grotzinger, S. Gupta, N. Lanza, S. Le Mouélic, S. Maurice, S.M. McLennan, P.-Y. Meslin, M. Nachon, H. Newsom, V. Payré, W. Rapin, M. Rice, V. Sautter, and A.H. Treiman, **The potassic sedimentary rocks in Gale Crater, Mars, as seen by ChemCam on board *Curiosity***, *Journal of Geophysical Research Planets*, 121(5):784-804, doi:10.1002/2015JE004987, 2016. [🕮]

Léveillé, R.J., J. Bridges, R.C. Wiens, N. Mangold, A. Cousin, N. Lanza, O. Forni, A. Ollila, J. Grotzinger, S. Clegg, K. Siebach, G. Berger, B. Clark, C. Fabre, R. Anderson, O. Gasnault, D. Blaney, L. Deflores, L. Leshin, S. Maurice, and H. Newsom, **Chemistry of fracture-filling raised ridges in Yellowknife Bay, Gale Crater: Window into past aqueous activity and habitability on Mars**, *Journal of Geophysical Research Planets*, 119 (11):2398-2415, doi:10.1002/2014JE004620, 2014. [🕮]

Mahaffy, P.M., C.R. Webster, M. Cabane, P.C. Conrad, P. Coll, S.K. Atreya, R. Arvey, M. Barciniak, M. Benna, L. Bleacher, W.B. Brinckerhoff, J.L. Eigenbrode, D. Carignan, M. Cascia, R.A. Chalmers, J.P. Dworkin, T. Errigo, P. Everson, H. Franz, R. Farley, S. Feng, G. Frazier, C. Freissinet, D.P. Glavin, D.N. Harpold, D. Hawk, V. Holmes, C.S. Johnson, A. Jones, P. Jordan, J. Kellogg, J. Lewis, E. Lyness, C.A. Malespin, D.K. Martin, J. Mauren, A.C. McAdam, D. McLennan, T.J. Nolan, M. Noriega, A.A. Pavlov, B. Prats, E. Raaen, O. Sheinman, D. Sheppard, J. Smith, J.C. Stern, F. Tan, M. Trainer D.W. Ming, R.V. Morris, J. Jones, C. Gundersen, A. Steele, J. Wray, O. Botta, L.A. Leshin, T. Owen, S. Battel, B.M. Jakosky, H. Manning, S. Squyres, R. Navarro-González, C.P. McKay, F. Raulin, R. Sternberg, A. Buch, P. Sorensen, R. Kline-Schoder, D. Coscia, C. Szopa, S. Teinturier, C. Baffes, J. Feldman, G. Flesch, S. Forouhar, R. Garcia, D. Keymeulen, S. Woodward, B.P. Block, K. Arnett, R. Miller, C. Edmonson, S. Gorevan, and E. Mumm, **The Sample Analysis at Mars investigation and instrument suite**, *Space Science Reviews*, 170:401-478, doi:10.1007/s11214-012-9879-z, 2012. [🔓]

Mahaffy, P.R., C.R. Webster, J.C. Stern, A.E. Brunner, S.K. Atreya, P.G. Conrad, S. Domagal-Goldman, J.L. Eigenbrode, G.J. Flesch, L.E. Christensen, H.B. Franz, C. Freissinet, D.P. Glavin, J.P Grotzinger, J.H. Jones, L.A. Leshin, C. Malespin, A.C. McAdam, D.W. Ming, R. Navarro-Gonzalez, P.B. Niles, T. Owen, A.A. Pavlov, A. Steele, M.G. Trainer, K.H. Williford, J.J. Wray, and the MSL Science Team, **The imprint of atmospheric evolution in the D/H of Hesperian clay minerals on Mars**, *Science*, 347(6220):412-414, doi:10.1126/science.1260291, 2015. [🔓] [🔓] [🕮]

© 2016 American Geophysical Union. All rights reserved.

McDougall I. and Harrison T.M. **Geochronology and Thermochronology by the $^{40}Ar/^{39}Ar$ Method** (2nd edition). Oxford University Press, New York, 1999.

Nachon, M., S.M. Clegg, N. Mangold, S. Schröder, L.C. Kah, G. Dromart, A. Ollila, J.R. Johnson, D.Z. Oehler, J.C. Bridges, S. Le Mouélic, O. Forni, R.C. Wiens, R.B. Anderson, D.L. Blaney, J.F. Bell III, B. Clark, A. Cousin, M.D. Dyar, B. Ehlmann, C. Fabre, O. Gasnault, J. Grotzinger, J. Lasue, E. Lewin, R. Léveillé, S. McLennan, S. Maurice, P.-Y. Meslin, W. Rapin, M. Rice, S.W. Squyres, K. Stack, D.Y. Sumner, D. Vaniman, and D. Wellington, **Calcium sulfate veins characterized by ChemCam/Curiosity at Gale Crater, Mars**, *Journal of Geophysical Research Planets*, 119(9):1991-2016, doi:10.1002/2013JE004588, 2014. [🕮]

Pavlov, A. A.; Vasilyev, G.; Ostryakov, V. M.; Pavlov, A. K.; Mahaffy, P.: Degradation of the organic molecules in the shallow subsurface of Mars due to irradiation by cosmic rays. Geophys. Res. Lett. 2012, 39, 13202.

Pecora, W.T. **Nepheline syenite pegmatites, Rocky Boy Stock, Bearpaw Mountains, Montana**, *The American Mineralogist*, 27(6), 1942.

Renne. P.L., Mundil, R., Balco, G., Min, K., and Ludwig, K.R. **Joint determination of ^{40}K decay constants and $^{40}Ar^*/^{40}K$ for the Fish Canyon sanidine standard, and improved accuracy for $^{40}Ar/^{39}Ar$ geochronology**, *Geochim. Cosmochim. Acta* **75**, 5097–5100, doi:10.1016/j.gca.2011.06.021, 2010.

Thompson, L.M., M.E. Schmidt, J.G. Spray , J.A. Berger , A.G. Fairén , J.L. Campbell , G.M. Perrett , N. Boyd , R. Gellert , I. Pradler , and S.J. VanBommel, **Potassium- rich sandstones within the Gale impact crater, Mars: The APXS perspective**, *Journal of Geophysical Research Planets*, 121, doi:10.1002/2016JE005055, in press. [🕮]

Treiman et al., **Mineralogy and genesis of the Windjana sandstone, Kimberley area, Gale Crater, Mars.** *46th Lunar and Planetary Science Conference (2015)* 2620.pdf, 2015.

Treiman, A. H., et al. (2016), Mineralogy, provenance, and diagenesis of a potassic basaltic sandstone on Mars: CheMin X-ray diffraction of the Windjana sample (Kimberley area, Gale Crater), J. Geophys. Res. Planets, 121, doi:10.1002/2015JE004932.

Vaniman, D.T., D.L. Bish, D.W. Ming, T.F. Bristow, R.V. Morris, D.F. Blake, S.J. Chipera, S.M. Morrison, A.H. Treiman, E.B. Rampe, M. Rice, C.N. Achilles, J.P. Grotzinger, S.M. McLennan, J. Williams, J.F. Bell III, H.E. Newsom, R.T. Downs, S. Maurice, P. Sarrazin, A.S. Yen, J.M. Morookian, J.D. Farmer, K. Stack, R.E. Milliken, B.L. Ehlmann, D.Y. Sumner, G. Berger, J.A. Crisp, J.A. Hurowitz, R. Anderson, D.J. Des Marais, E.M. Stolper, K.S. Edgett, S. Gupta, N. Spanovich, and MSL Science Team, **Mineralogy of a mudstone at Yellowknife Bay, Gale Crater, Mars**, *Science*, 343(6169), 1243480, doi:10.1126/science.1243480, 2014. [🔓] [🔓] [🕮]

Vasconcelos, P. M., **K-Ar and $^{40}Ar/^{39}Ar$ geochronology of weathering processes**, *Annu. Rev. Earth Pl. Sc., 27*, 183-229, doi:10.1146/annurev.earth.27.1.183, 1999.

© 2016 American Geophysical Union. All rights reserved.

Waltenberg, K.M., **Mineral Physics and crystal chemistry of minerals suitable for weathering geochronology: implications to $^{40}Ar/^{39}Ar$ and (U-Th)/He geochronology**. PhD Thesis, School of Earth Sciences, The University of Queensland, pp. 421, 2012.

Woodard, H.H., **Syngenetic sanidine beds from Middle Ordovician Saint Peter sandstone, Wisconsin**, *The Journal of Geology*, 80(3): 323-332, 1972.

© 2016 American Geophysical Union. All rights reserved.

List of Figures

© 2016 American Geophysical Union. All rights reserved.

1. Stabilized Interval for Windjana 1, m/z 2 and 3
2. M/z 2 vs 3 correlation
3. Stabilized Interval for Windjana 1, m/z 20 and 21
4. M/z 20 vs 21 correlation
5. Stabilized Interval for Windjana 1, m/z 36 and 38 for ^{36}Ar calculation

Figure 8 – Windjana 2 (WJ2) ^{3}He, ^{21}Ne, and ^{36}Ar Analyses

1. Stabilized Interval for Windjana 2, m/z 2 and 3
2. M/z 2 vs 3 correlation
3. Stabilized Interval for Windjana 2, m/z 20 and 21
4. M/z 20 vs 21 correlation
5. Stabilized Interval for Windjana 2, m/z 36 and 38 for ^{36}Ar calculation

© 2016 American Geophysical Union. All rights reserved.

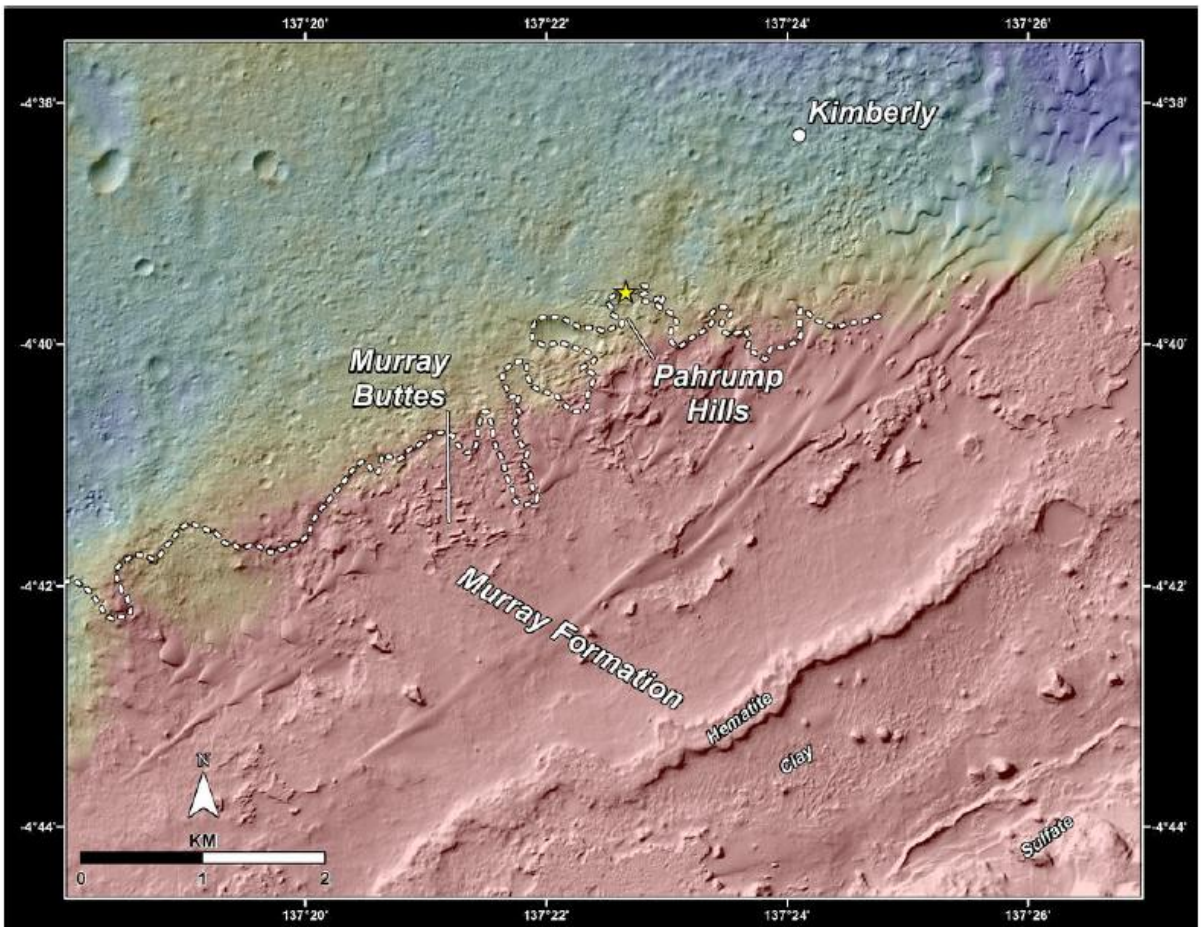

Figure 1 – The geological map (a) and topographic profile (b) for the units visited and sampled during the rover traverse from the landing site at Yellowknife Bay to the base of Mount Sharp illustrates the sites sample for chemical, mineralogical, and isotopic studies, including the Windjana outcrop investigated in this study (from Grotzinger et al., 2012, 2015).

© 2016 American Geophysical Union. All rights reserved.

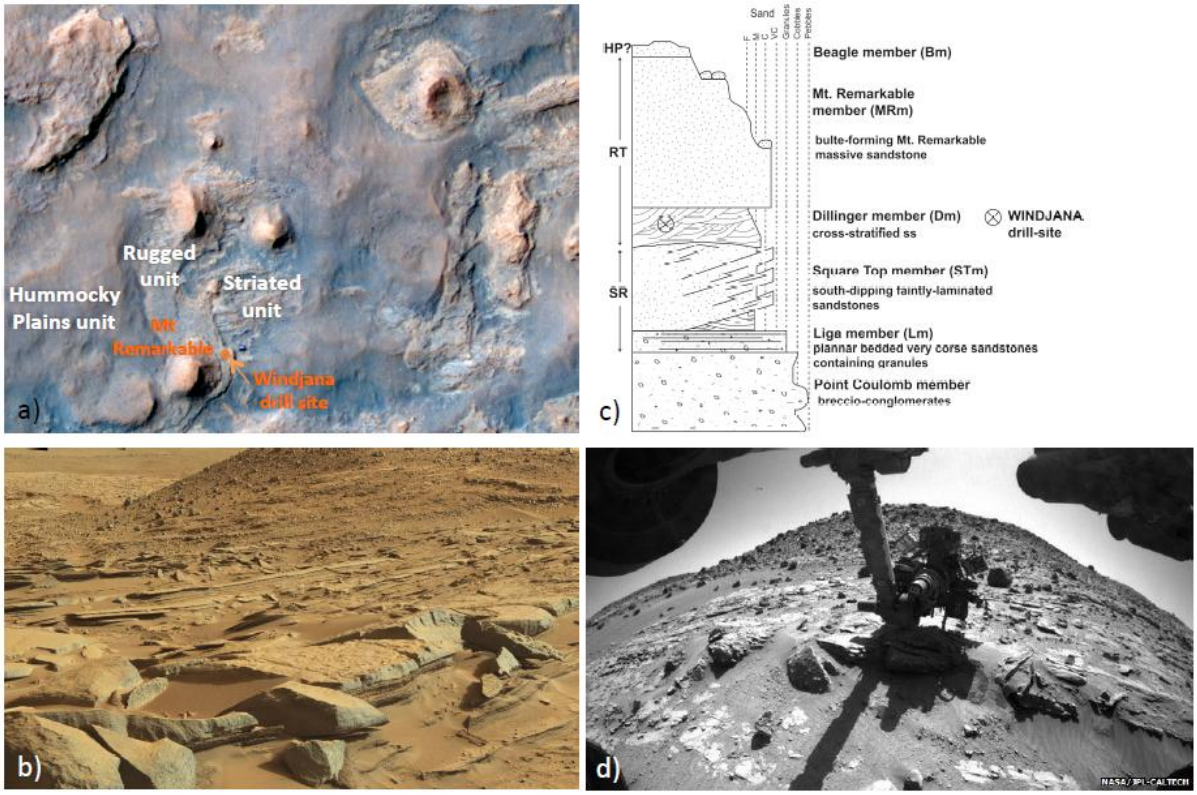

Figure 2 – (a) HiRISE IRB color image showing the Curiosity rover at the base of Mt Remarkable and next to the outcrops of the Dillinger member (DM) of the Kimberley formation. A stratigraphic section (after Le Deit et al. 2015) for the units exposed at Mt Remarkable illustrate the sedimentary context of cross-bedded sandstone sampled for geochronology. The cross-bedded sandstone slabs selected for drilling is shown in [c) and [d) illustrates the drilling campaign with Mt Remarkable in the background.

© 2016 American Geophysical Union. All rights reserved.

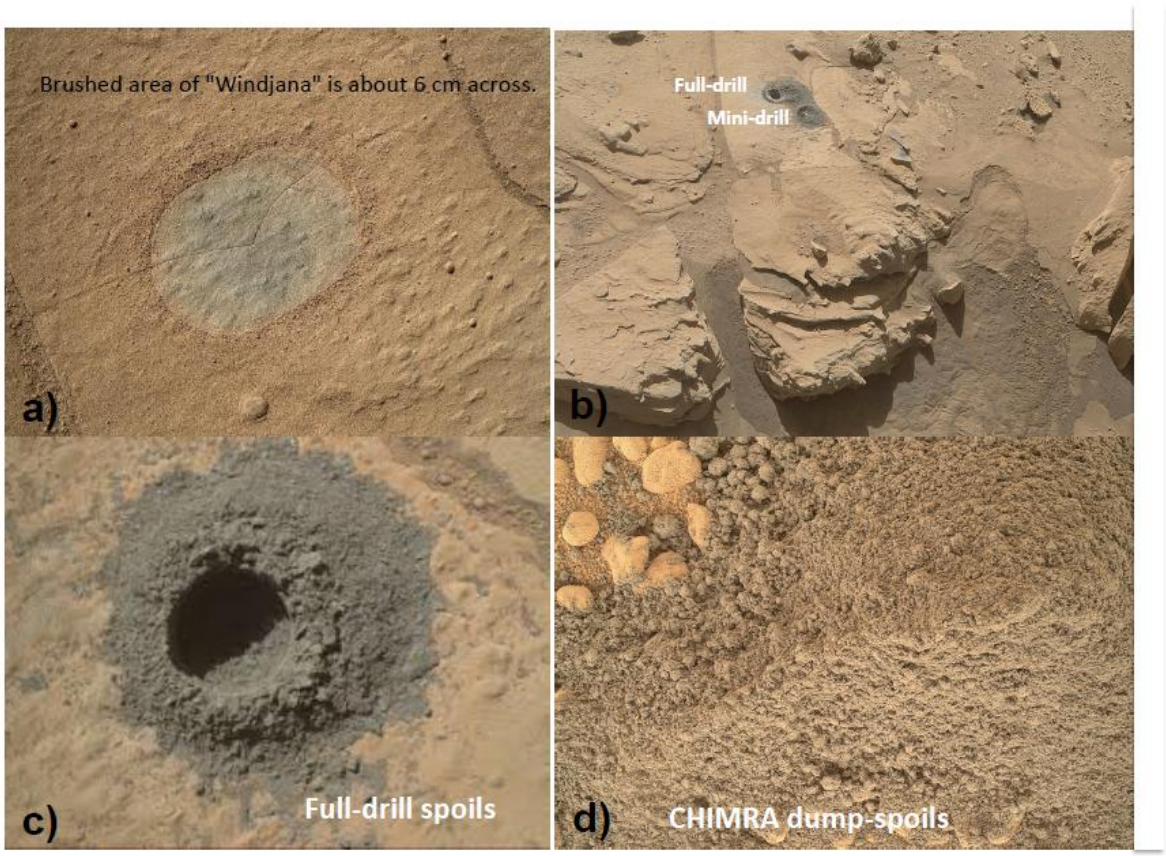

Figure 3 – (a) Mars Hand Lens Imager (Mahli) shows the area selected for full-drill, illustrating the granular nature of the sediments, a fracture cross-cutting the drilling spot, and the darker nature of the brushed sediments after removal of the dust cover. MAHLI images for the mini- and full-drill sites (b) and spoils (c-d) illustrate the darker and coarser grained nature of the sediments drilled at Windjana when compared to sediments drilled for geochronology at Cumberland [Farley et al, 2014].

© 2016 American Geophysical Union. All rights reserved.

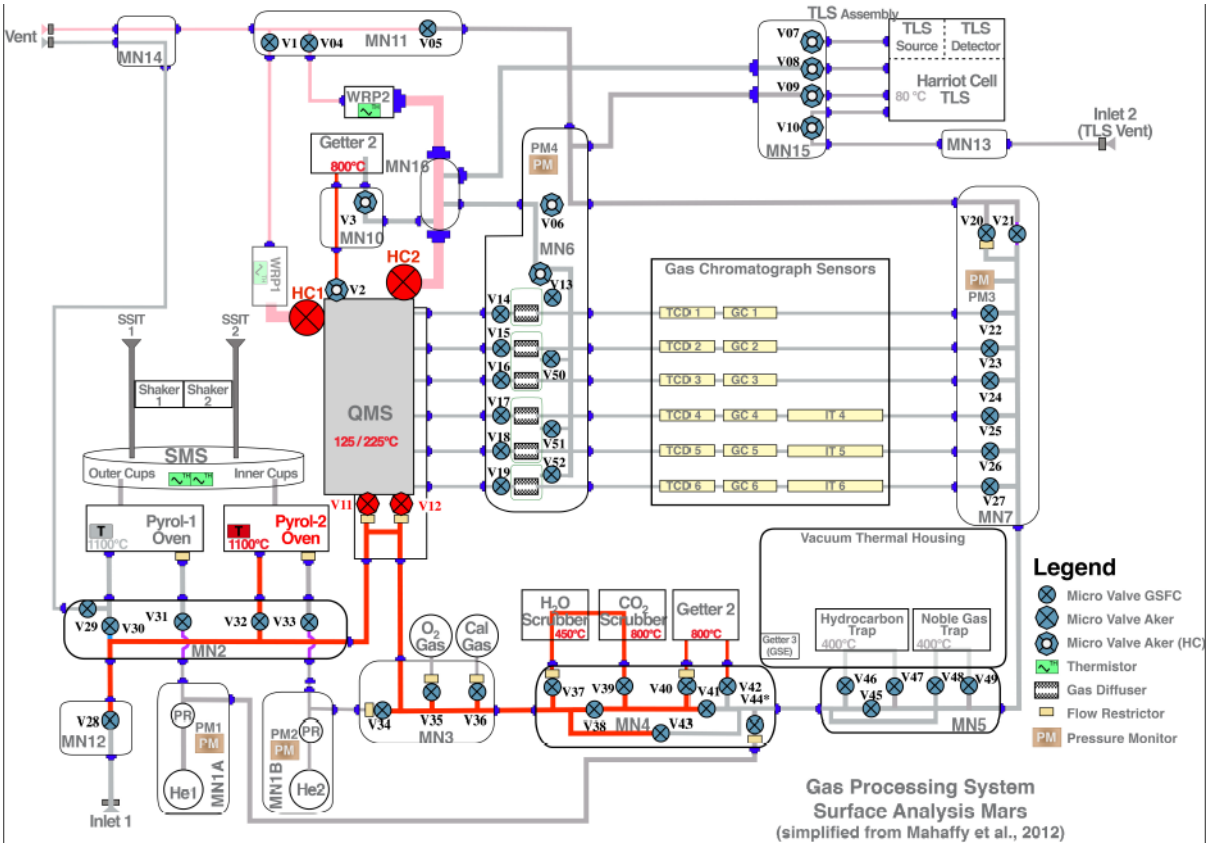

Figure 4 – The Gas Processing System in the SAM (Surface Analysis Mars) mini-laboratory illustrates the complex array of instruments and analytical versatility provided by the Curiosity rover instruments. In the three (WJ1, WJ1-RE, and WJ2) experiments, the sample aliquots were heated in Pyrol-2 Oven, and the sample gases were cleaned through the segment of the instrument illustrated in red and analyzed in dynamic (HC1 and HC2 opened) and semi-static modes (HC1 and HC2 partially closed), as discussed in the text.

© 2016 American Geophysical Union. All rights reserved.

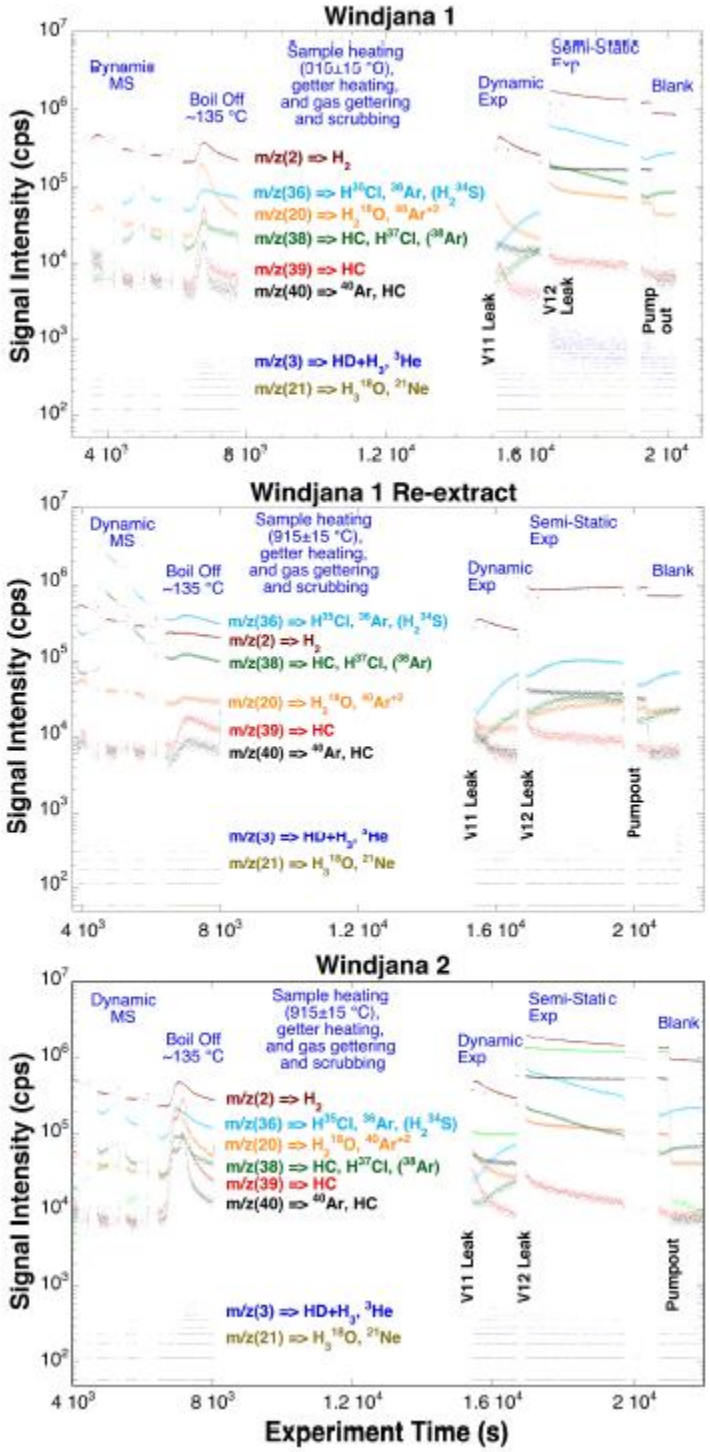

Figure 5 – (a), (b) and (c) illustrate the evolution of gases of selected masses (m/z = 2, 3, 20, 21, 36, 38, 39, and 40) important for the geochronology experiments discussed here. Gas analysis before sample heating, during the boil off period, and during the dynamic, semi-static, pump-out, and background [blank) analyses illustrate the relative abundances and distinct behavior between noble and active gases during the analytical procedure.

© 2016 American Geophysical Union. All rights reserved.

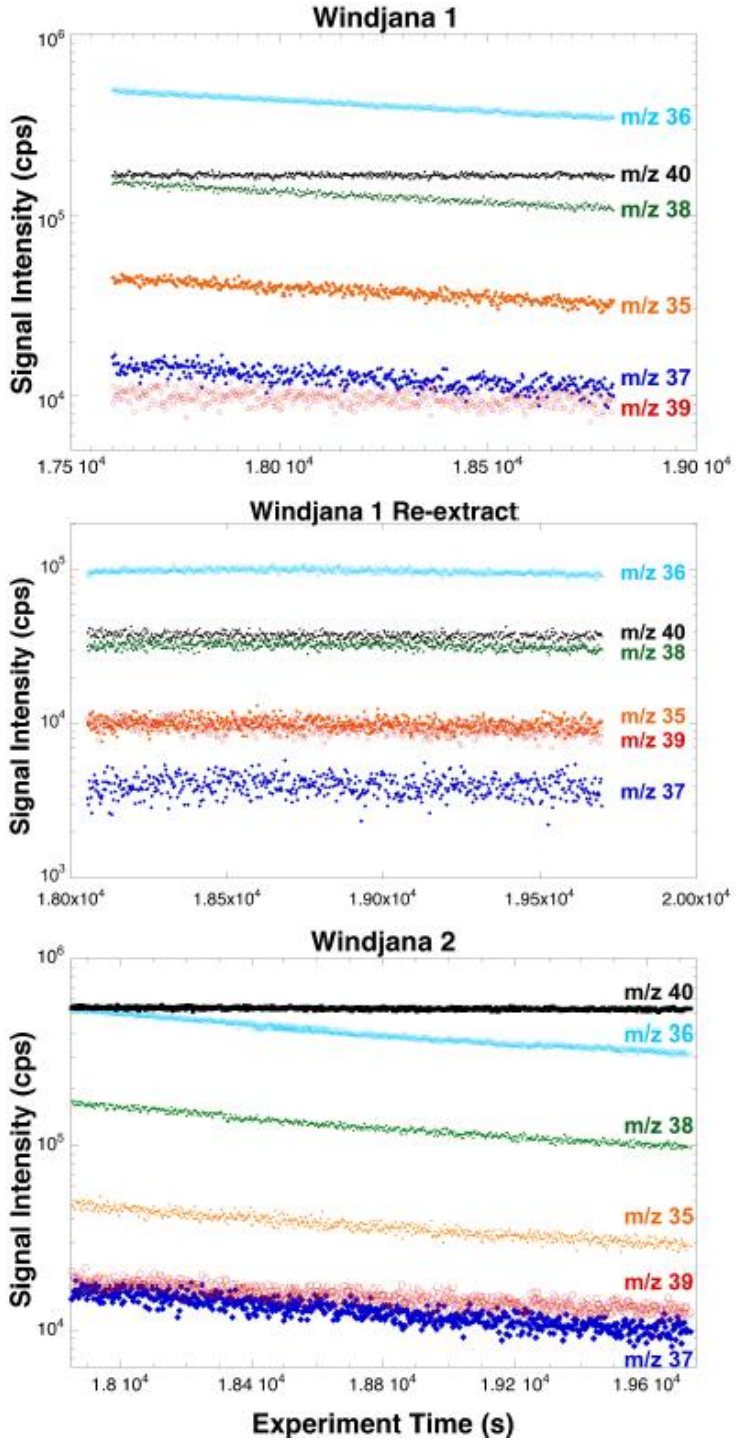

Figure 6 – Gas concentrations during the semi-static stabilized periods for samples WJ1, WJ1-RE, and WJ2 illustrate the relative concentrations of the m/z of interest for age calculation. It is important to notice that m/z dominated by noble gases (M40) remains constant throughout the experiment, where active species (e.g., M38) undergo depletion during analysis, except for the WJ1_RE experiment, where relatively invariant concentrations suggest that the species investigated were only present at background levels. Quantification of each m/z is described in greater detail in the text and in Farley et al. [2014].

© 2016 American Geophysical Union. All rights reserved.

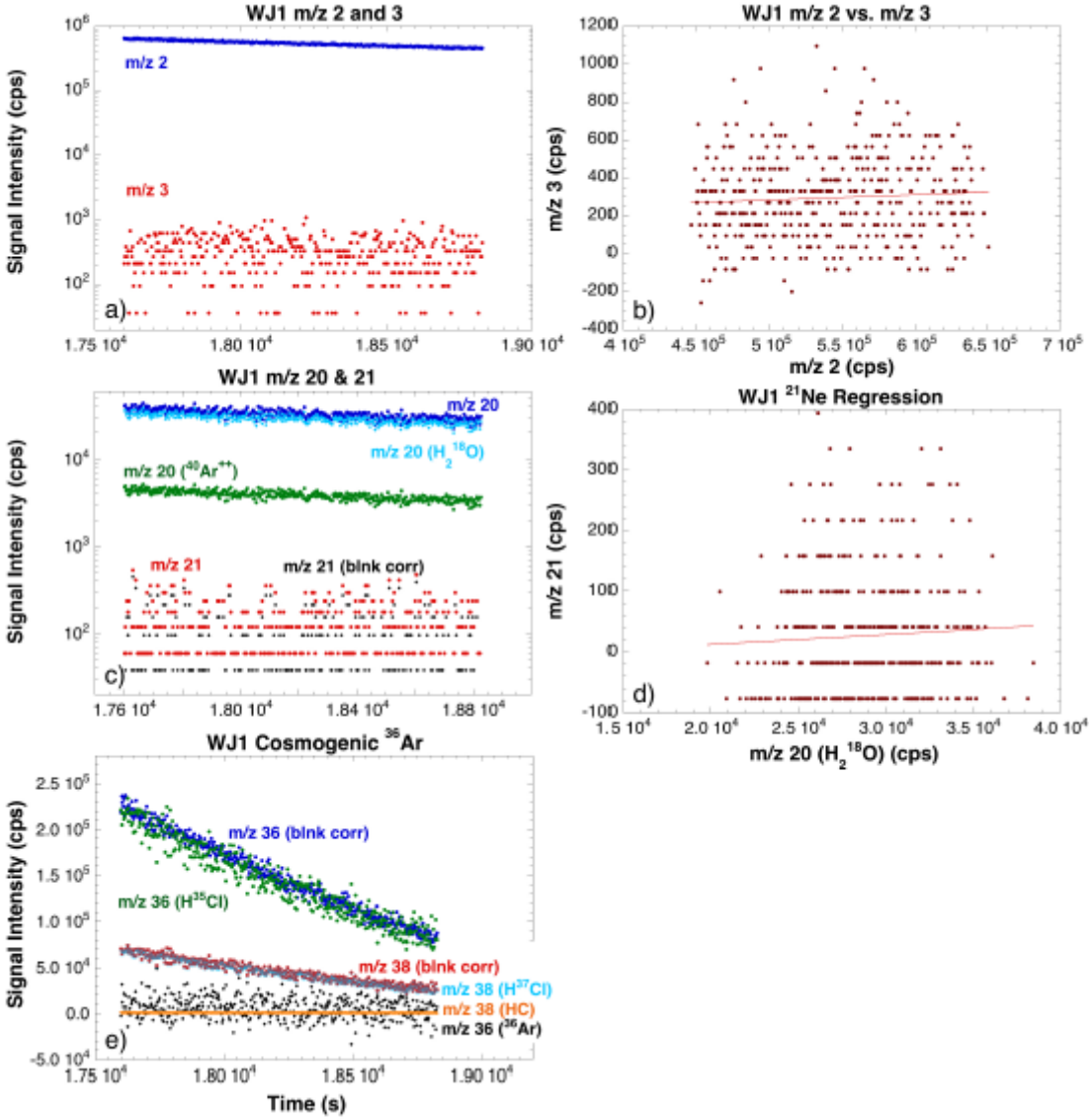

Figure 7 – Gas concentrations (a, c, and e) and correlations (b and d) used in the quantification of cosmogenic noble gases (^{3}He, ^{21}Ne, and ^{36}Ar), according to the procedures outlined in Farley et al. [2014], for the WJ1 experiments.

© 2016 American Geophysical Union. All rights reserved.

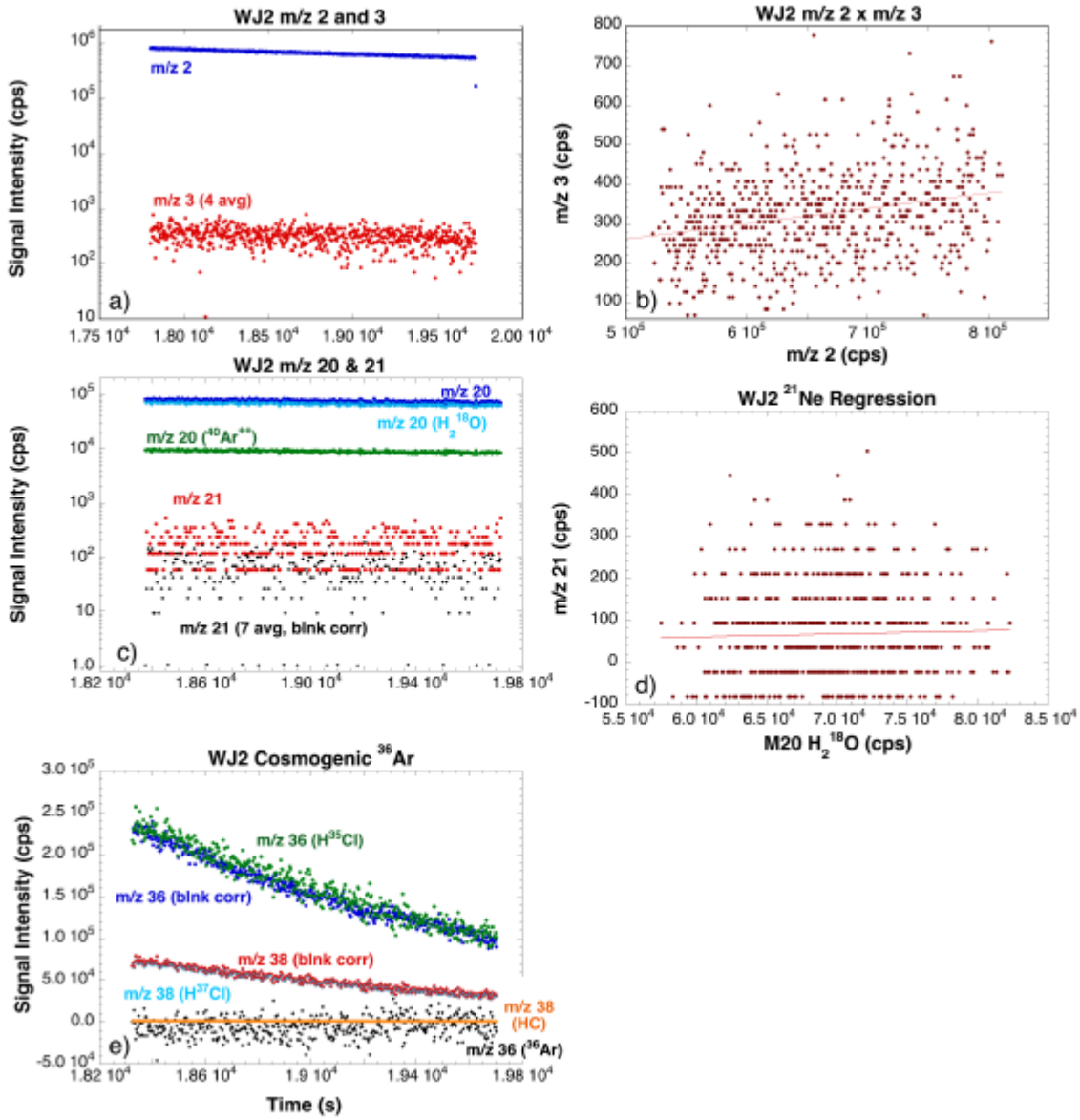

Figure 8 – Gas concentrations (a, c, and e) and correlations (b and d) used in the quantification of cosmogenic noble gases (^{3}He, ^{21}Ne, and ^{36}Ar), according to the procedures outlined in Farley et al. [2014], for the WJ2 experiments.

© 2016 American Geophysical Union. All rights reserved.

Table 1. APXS Chemical Analyses of the Windjana sandstone fraction relevant for the geochronology experiments (from Treiman et al., 2016).

Sol	704	
Wt %	DumpPile	± 2σ
SiO_2	37.38	0.86
TiO_2	1.07	0.06
Al_2O_3	5.62	0.38
Cr_2O_3	0.49	0.02
FeO	27.90	0.66
MnO	0.53	0.02
MgO	12.29	0.50
CaO	5.26	0.12
Na_2O	0.96	0.14
K_2O	3.09	0.20
P_2O_5	0.64	0.10
SO_3	3.57	0.10
Cl	0.57	0.02
Total	99.37	
Ni ppm	516	30
Zn ppm	4775	145
Br ppm	123	5

© 2016 American Geophysical Union. All rights reserved.

Table 2. Mass Proportions of Phases in the Windjana Sandstone (from Treiman et al., 2016).

Mineral	Windjana Mass % Crystalline	Windjana Mass % Total
Sanidine	27(5)	20(3)
Oligoclase	3.0(5)	2.0(5)
Labradorite	det	det
Andesine	2(2)	2(2)
Plagioclase Total	5(2)	4(2)
Olivine	7.2(7)	5.4(5)
Augite	26(4)	20(3)
Pigeonite	13.5(25)	10(2)
Enstatite	det	det
Magnetite	16(3)	12.4(15)
Ilmenite	1.0(4)	0.8(5)
Hematite	1.2(4)	1.0(3)
Pyrrhotite	0.6(6)	0.5(5)
Akaganeite	0.4(3)	0.3(2)
Anhydrite	0.5(5)	0.5(5)
Bassanite	0.8(3)	0.7(3)
Jarosite	det	det
Fluorapatite	1.7(8)	1.3(6)
Quartz	-	-
Halite	-	-
Pyrite	-	-
Kaolinite	1(1)	det
Smectite/Illite	-	10
Amorphous	-	15

© 2016 American Geophysical Union. All rights reserved.

Table 3 – K-Ar and exposure age calculations for WJ1, WJ1-RE, and WJ2, using the chemical compositions listed in Table 2 and the sample mass (135 ± 18 mg) estimated as described in the text. Production rates for cosmogenic ^{3}He, ^{21}Ne, and ^{36}Ar are estimated from the compositions listed in Table 2 and the model of Farley et al. [2014].

Windjana Sandstone Windjana 1 (WJ1)

Sample Mass 0.135 ± 0.018 g

K-Ar System		±1σ
K_2O (wt %)	3.09	0.20
^{40}Ar (pmol/g)	3264	25
K-Ar Age (Ma)	627	50

Cosmogenic Isotopes

			PR (pmol g^{-1} Ma^{-1})[A]		Exposure Age[B]	
Isotope	pmol/g	±1σ	Surface	2m Average	(Ma)	±1σ
^{3}He	24.8	21.2	0.4333	0.1631	57	49
^{21}Ne	0.12	1.73	0.0518	0.0234	2	32
^{36}Ar	26.5	41.9	0.0139	0.0071	65	104

Windjana Sandstone Windjana 2 (WJ2)

Sample Mass 0.135 ± 0.018 g

K-Ar System		±1σ
K_2O [wt %)	3.09	0.20
^{40}Ar [pmol/g)	12404	25
K-Ar Age [Ma)	1710	110

Cosmogenic Isotopes

			PR (pmol g^{-1} Ma^{-1})[A]		Exposure Age[B]	
Isotope	pmol/g	±1σ	Surface	2m Average	(Ma)	±1σ
^{3}He	7.7	13.9	0.4333	0.1631	18	32
^{21}Ne	4.53	1.30	0.0518	0.0234	83	24
^{36}Ar	24.1	58.4	0.0139	0.0071	60	144

Notes: elemental composition from APXS measurement of ingested and subsequently dumped Windjana.

[A]- model isotope production rate [Farley et al., 2014].

[B]- surface exposure age assuming no erosion.

© 2016 American Geophysical Union. All rights reserved.